Reprinted from



JOURNAL OF CRYSTAL GROWTH

Journal of Crystal Growth 171 (1997) 288–302

# Buoyancy-driven heat transfer during application of a thermal gradient for the study of vapor deposition at low pressure using an ideal gas

D.O. Frazier [a,*], R.J. Hung [b], M.S. Paley [c], B.G. Penn [a], Y.T. Long [b]

[a] *Space Sciences Laboratory, NASA Marshall Space Flight Center, Huntsville, Alabama 35812, USA*
[b] *Department of Mechanical and Aerospace Engineering, University of Alabama in Huntsville, Huntsville, Alabama 35899, USA*
[c] *Universities Space Research Association, Space Sciences Laboratory, NASA Marshall Space Flight Center, Huntsville, Alabama 35812, USA*

Received 23 February 1996; accepted 27 June 1996

ELSEVIER

# Journal of Crystal Growth



**Scope of the Journal**
Experimental and theoretical contributions are invited in the following fields: Theory of nucleation and growth, molecular kinetics and transport phenomena, crystallization in viscous media such as polymers and glasses. Crystal growth of metals, minerals, semiconductors, magnetics, inorganic, organic and biological substances in bulk or as thin films. Apparatus, instrumentation and techniques for crystal growth, and purification methods. Characterization of single crystals by physical and chemical methods.


**Abstracted/Indexed in:**
Aluminium Industry Abstracts; Chemical Abstracts; Current Contents: Physical, Chemical and Earth Sciences; EI Compendex Plus; Engineered Materials Abstracts; Engineering Index; INSPEC; Metals Abstracts.

**Subscription Information 1997**
Volumes 170–181 of Journal of Crystal Growth (ISSN 0022-0248) are scheduled for publication. (Frequency: semimonthly.) Prices are available from the publishers upon request. Subscriptions are accepted on a prepaid basis only. Issues are sent by SAL (Surface Air Lifted) mail wherever this service is available. Airmail rates are available upon request. Please address all enquiries regarding orders and subscriptions to:

Elsevier Science B.V., Order Fulfilment Department
P.O. Box 211, 1000 AE Amsterdam, The Netherlands
Tel: +31 20 485 3642; Fax: +31 20 485 3598

Claims for issues not received should be made within six months of our publication (mailing) date.

**US mailing notice** - *Journal of Crystal Growth* (ISSN 0022-0248) is published semimonthly by Elsevier Science B.V., Molenwerf 1, P.O. Box 211, 1000 AE Amsterdam, The Netherlands. Annual subscription price in the USA is US $7081 (valid in North, Central and South America only), including air speed delivery. Periodicals postage paid at Jamaica NY 11431.
US postmasters: Send address changes to Journal of Crystal Growth, Publications Expediting, Inc., 200 Meacham Avenue, Elmont NY 11003. Airfreight and mailing in the USA by Publications Expediting.

The paper used in this publication meets the requirements of ANSI/NISO Z39.48-1992 (Permanence of Paper)

PRINTED IN THE NETHERLANDS

North-Holland, an imprint of Elsevier Science

ELSEVIER

Journal of Crystal Growth 171 (1997) 288–302

JOURNAL OF CRYSTAL GROWTH

# Buoyancy-driven heat transfer during application of a thermal gradient for the study of vapor deposition at low pressure using an ideal gas

D.O. Frazier [a,*], R.J. Hung [b], M.S. Paley [c], B.G. Penn [a], Y.T. Long [b]

[a] *Space Sciences Laboratory, NASA Marshall Space Flight Center, Huntsville, Alabama 35812, USA*

[b] *Department of Mechanical and Aerospace Engineering, University of Alabama in Huntsville, Huntsville, Alabama 35899, USA*

[c] *Universities Space Research Association, Space Sciences Laboratory, NASA Marshall Space Flight Center, Huntsville, Alabama 35812, USA*

Received 23 February 1996; accepted 27 June 1996

**Abstract**

A mathematical model has been developed to determine heat transfer during vapor deposition of source materials under a variety of orientations relative to gravitational accelerations. The model demonstrates that convection can occur at total pressures as low as $10^{-2}$ mm Hg. Through numerical computation, using physical material parameters of air, a series of time steps demonstrates the development of flow and temperature profiles during the course of vapor deposition. These computations show that in unit gravity vapor deposition occurs by transport through a fairly complicated circulating flow pattern when applying heat to the bottom of the vessel with parallel orientation with respect to the gravity vector. The model material parameters for air predict the effect of kinematic viscosity to be of the same order as thermal diffusivity, which is the case for Prandtl number $\sim 1$ fluids. Qualitative agreement between experiment and the model indicates that 6-(2-methyl-4-nitroanilino)-2,4-hexadiyn-1-ol (DAMNA) at these pressures indeed approximates an ideal gas at the experiment temperatures, and may validate the use of air physical constants. It is apparent that complicated nonuniform temperature distribution in the vapor could dramatically affect the homogeneity, orientation, and quality of deposited films. The experimental test is a qualitative comparison of film thickness using ultraviolet-visible spectroscopy on films generated in appropriately oriented vapor deposition cells. In the case where heating of the reaction vessel occurs from the top, deposition of vapor does not normally occur by convection due to a stable stratified medium. When vapor deposition occurs in vessels heated at the bottom, but oriented relative to the gravity vector between these two extremes, horizontal thermal gradients induce a complex flow pattern. In the plane parallel to the tilt axis, the flow pattern is symmetrical and opposite in direction from that where the vessel is positioned vertically. The ground-based experiments are sufficient preliminary tests of theory and should be of significant interest regarding vapor deposited films in microgravity.

## 1. Introduction

In recent years, a great deal of interest has been directed toward the use of organic materials in the development of higher efficiency optoelectronic devices. There is a myriad of possibilities among organics which allow flexibility in the design of unique structures with a variety of functional group objectives. The use of nonlinear optical (NLO) organic materials such as thin film waveguides allows full

* Corresponding author. Fax: + 1 205 544 2102.


*PII* S0022-0248(96)00500-3

exploitation of their desirable qualities by permitting long interaction lengths and large power densities with modest power input [1]. There are several methods in use to prepare thin films, such as Langmuir–Blodgett [2–4], growth from sheared solution or melt [5,6], and melt growth between glass plates [7].

Epitaxial growth on ordered organic and inorganic substrates and variations in processing conditions have been useful for preparing highly oriented polydiacetylene (PDA) and phthalocyanine (Pc) films [8–10]. The degree of significance relating processing conditions to uniformity in thickness, degree of orientation, and optical properties for a specific processing technique is the general focus of the work of the research group at the Marshall Space Flight Center (MSFC). A study on the effect of processing conditions relevant to thin film deposition by physical vapor transport (PVT) is particularly difficult because of the possibility that convection may play a major role. It is a goal of some researchers having an interest in PVT to produce good quality anisotropic films, therefore, an important yet understudied requirement should be to assess the role of gravity during processing. This may be particularly true for the vapor deposition of diacetylenes where subsequent polymerization in the crystal is topochemical and occurs readily only when neighboring monomer molecules are sufficiently close and suitably oriented [11]. Likewise, this requirement is equally viable for the vapor deposition of Pc's in view of the results of microgravity experiments by the 3M Corporation involving the preparation of thin films of copper Pc (CuPc) [12–22]. Indeed, a variety of microstructural forms were obtained in thin films of CuPc dependent on processing methods and conditions. Small changes in processing parameters caused large changes in film orientation. Microgravity grown CuPc had several desirable features, which indicate that the growth of organic films in low-$g$ may result in better quality films for optical and electrical applications [21,22]. The dramatic 3M result was generally unexpected and has been the source of considerable discussion over the 4–6 years since the performance of these experiments.

At MSFC, we have begun studying the thin film growth of metal-free Pc [23], CuPc, and a polymerized 2-methyl-4-nitroaniline diacetylene derivative (PDAMNA) [8,24]. Experimentation on the deposition of these materials include PVT processing, although the conditions at which transport occurs differ considerably between the various materials. The deposition of the diacetylene monomer (DAMNA) occurred at a pressure of $10^{-2}$ mm Hg. Most arguments, usually of a qualitative nature, suggest that convection is not a factor at pressures below about 10 mm Hg, because momentum transfer is arguably minimal due to large mean free paths. This would suggest that most processes could be designed to operate at low enough pressures as to negate orientational and other possible gravitationally sensitive effects. Secondarily, our purpose is to begin a systematic experimental and theoretical study to determine a range of pressure thresholds for which one would need to be concerned with convection. For Pc, the 3M method [9] involved deposition of metal-free Pc as substrate on the ground at about $10^{-6}$ mm Hg. At these very low pressures, orientation of the molecular $b$-axis was only a function of temperature with no gravitational dependence. Epitaxial growth of CuPc at much higher pressures onto the metal-free substrate required the low gravity environment for maximum orientation of the CuPc film (PVT for organic solids (PVTOS)).

A major goal of our research program is to understand factors for improving film quality and optical properties in vapor deposited films. Important aspects of any study involving fluids, as in vapor transport, are driving mechanisms for heat transfer with natural convection and diffusion processes which determine flow profiles and temperature distributions. In this study, we have considered initiation and development of time-dependent, three-dimensional fluctuations of flow profiles and temperature distribution. These phenomena are driven by heat transfer in parallel and oblique directions with respect to gravitational acceleration. Furthermore, consideration of pressure effects suggest that in unit gravity, convection can occur at lower pressures than previously thought. The ground-based portion of this study investigates factors influencing vapor transport varying reactor orientation with respect to the gravity vector. We seek to correlate cell orientation and other processing parameters with film quality. Extensive experimental and theoretical work will provide data to assess the value of future microgravity processing. The primary objective of this work, how-

ever, is to concentrate on the theoretical framework which describes heat flow and thermal profiles using time-dependent, three-dimensional formulations at various cell orientations. Tests of theoretical predictions initially rely on relative film thickness measurements following depositions in appropriately positioned cells.

Recognizing the criticality of selected boundary conditions, the size and geometry of the container in these simulations represent initial parameters and define actual but roughly designed ground-based experiments. The results of this study will allow refinement of cell dimensions and design for assessment of past and future ground-based work, and provide an additional basis for investigating microgravity processing by PVT.

## 2. Mathematical formulation

In this section, we introduce the governing equations, initial and boundary conditions to assess the flow fields and temperature distributions upon application of a thermal gradient to an ideal gas. There is no species diffusion component to the formulation that accounts for boundary fluxes driven by sublimation at the source and condensation at the sink [24–26]. Subsequent computations will contain species diffusion equations with inclusion of advective-diffusion flow. These computations approach steady state and for unit gravity, time-dependent flows and temperature distributions generally result from initial transients.

We did not seek to observe oscillatory flows. Time-dependent computations during microgravity processing, however, can serve the important purpose of correlating experimental results with fluctuating accelerometer data. Subsequent computations will explore time-dependent oscillatory flow behavior with Fourier component analyses for both unit and microgravity environments.

Consider a coaxial cylinder with an inner radius of $R_1$ and an outer radius of $R_2$. The heights of the outer and inner cylinders are $L_2$, and $(L_2 - L_1)$, respectively. Fig. 1 shows the geometrical configuration of the coaxial cylinder. For the purpose of considering the mathematical formulation, we adopt cylindrical coordinates $(r,\theta,z)$ with corresponding velocity components $(u,v,w)$, and corresponding components of gravity acceleration $(g_r, g_\theta, g_z)$. Figs. 1a and 1b show the geometrical configuration of a coaxial cylinder in an $r$–$z$ plane and the $r$–$\theta$ plane,

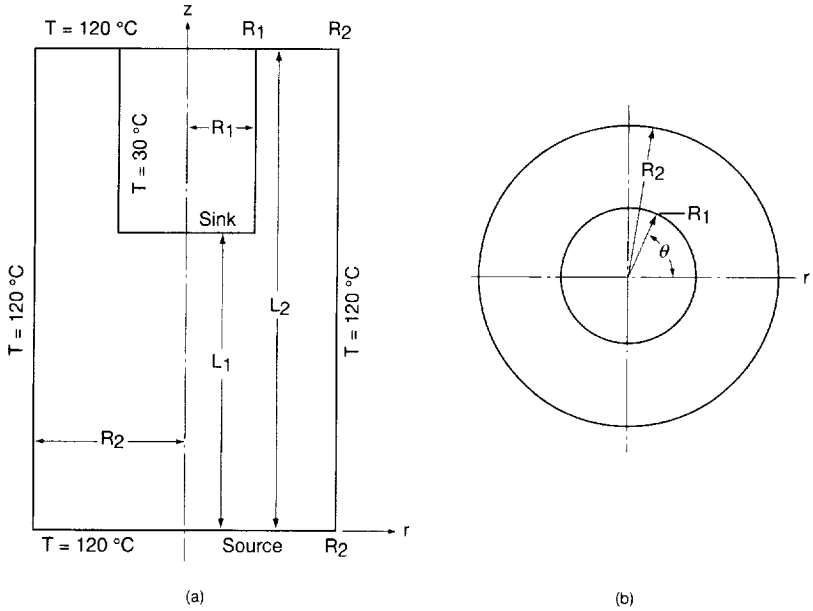


Fig. 1. Geometrical illustration of coaxial cylinders to be used for mathematical modeling, (a) an $r$–$z$ plane, and (b) the $r$–$\theta$ plane.

respectively. There are two temperature zones in this coaxial cylinder. During our growth of DAMNA films [27], the external walls of the outer cylinder are surrounded by an oil jacket, which maintains a constant temperature, ~ 120°C, while the walls of the inner cylinder keep a constant temperature of ~ 30°C. The cell, containing air, is evacuated to a pressure of $10^{-2}$ mm Hg (= 1.333 N/m$^2$). The air fills the gap between the outer and inner walls of the coaxial cylinder. The flow profiles and temperature distribution of the air in the cell at relatively low pressure are influenced by the natural convection of the flow pattern in this problem. The governing equations can be shown as follows:

Continuity equation,

$$\frac{1}{r}\frac{\partial}{\partial r}(ru) + \frac{1}{r}\frac{\partial v}{\partial \theta} + \frac{\partial w}{\partial z} = 0. \tag{1}$$

Momentum equations,

$$\rho\left(\frac{\partial u}{\partial t} + u\frac{\partial u}{\partial r} + \frac{v}{r}\frac{\partial u}{\partial \theta} - \frac{v^2}{r} + w\frac{\partial u}{\partial z}\right) = -\frac{\partial p}{\partial r} - \rho g_r[1 - \beta(T - T_\infty)] + \mu\left(\nabla^2 u - \frac{u}{r^2} - \frac{2}{r^2}\frac{\partial v}{\partial \theta}\right), \tag{2}$$

$$\rho\left(\frac{\partial v}{\partial t} + u\frac{\partial v}{\partial r} + \frac{v}{r}\frac{\partial v}{\partial \theta} + \frac{uv}{r} + w\frac{\partial v}{\partial z}\right) = -\frac{1}{r}\frac{\partial p}{\partial \theta} - \rho g_\theta[1 - \beta(T - T_\infty)] + \mu\left(\nabla^2 v - \frac{v}{r^2} + \frac{2}{r^2}\frac{\partial u}{\partial \theta}\right), \tag{3}$$

$$\rho\left(\frac{\partial w}{\partial t} + u\frac{\partial w}{\partial r} + \frac{v}{r}\frac{\partial w}{\partial \theta} + w\frac{\partial w}{\partial z}\right) = -\frac{\partial w}{\partial z} - \rho g_z[1 - \beta(T - T_\infty)] + \mu\nabla^2 w, \tag{4}$$

where

$$\beta = -\frac{1}{\rho_\infty}\left(\frac{\partial \rho}{\partial T}\right)_p,$$

$$\nabla^2 = \frac{1}{r}\frac{\partial}{\partial r}\left(r\frac{\partial}{\partial r}\right) + \frac{1}{r^2}\frac{\partial^2}{\partial \theta^2} + \frac{\partial^2}{\partial z^2},$$

and

$$(g_r, g_\theta, g_z) = g(\sin\psi\cos\theta, -\sin\psi\sin\theta, -\cos\psi).$$

Energy equation,

$$\rho c_p\left(\frac{\partial T}{\partial t} + u\frac{\partial T}{\partial r} + \frac{v}{r}\frac{\partial T}{\partial \theta} + w\frac{\partial T}{\partial z}\right) = k\nabla^2 T. \tag{5}$$

Here, $\rho$, $p$, $T$, $\mu$, $k$, and $g$ denote density, pressure, temperature, dynamic viscosity, thermal conductivity of air, and background gravity acceleration, respectively. $\psi$ is the angle between the gravity vector and the axis of the cylinder. In this case, $T_\infty$ and $\rho_\infty$ represent the air temperature and density at $10^{-2}$ mm Hg and heat sink at the wall of the inner cylinder at $T = 30$°C. In these mathematical expressions, the Boussinesq approximation is employed to formulate the relationship between local fluctuations of density and temperature through the thermal expansion coefficient which replaces the equation of state.

## 3. Initial and boundary conditions

The initial and boundary conditions have been assigned explicitly to solve governing Eqs. (1) to (5) simultaneously. The initial condition is at $t = 0$, all the flow profiles vanish, i.e.,

$$u = v = w = 0 \text{ everywhere.} \tag{6}$$

The temperature of fluid in the inner cylinder is 30°C. The temperature of fluid in the water jacket surrounding the outer cylinder is 120°C. These conditions are expressed by,

$$T = 30\text{°C at } r \le R_1,\ 0 \le \theta \le 2\pi,\ L_1 \le z \le L_2, \tag{7}$$

$$T = 120\text{°C at } z = 0;\ r \ge 0;\ 0 \le \theta \le 2\pi, \tag{8}$$

$$\text{at } z = L_2;\ r \ge 0;\ 0 \le \theta \le 2\pi, \tag{9}$$

$$\text{at } 0 \le z \le L_2;\ r = R_2;\ 0 \le \theta \le 2\pi. \tag{10}$$

The pressure profile inside the container at $t = 0$ is

$$p = 10^{-2}\ \text{mm Hg} = 1.333\ \text{N/m}^2. \tag{11}$$

The boundary conditions are that at time $t > 0$, the temperature distribution shown in Eqs. (7)–(10), and pressure profiles shown in Eq. (11) remain the

same. For flow profiles, no penetration and no slip conditions along the surfaces of the solid wall shall apply, namely,

$$u = v = w = 0 \tag{12}$$

along the surfaces of

$$r = R_1,\ 0 \le \theta \le 2\pi,\ L_1 \le z \le L_2, \tag{13}$$

$$r \ge 0,\ 0 \le \theta \le 2\pi,\ z = 0, \tag{14}$$

$$r \ge 0,\ 0 \le \theta \le 2\pi,\ z = L_2, \tag{15}$$

$$r = R_2,\ 0 \le \theta \le 2\pi,\ 0 \le z \le L_2. \tag{16}$$

The coaxial cylindrical container, in Fig. 1, has the following specifications: $L_1 = 6$ cm, $L_2 = 12$ cm, $R_1 = 0.9$ cm, and $R_2 = 1.5$ cm. The physical parameters for determining flow fields and temperature distribution were gravity acceleration $g_0 = 9.81$ m/s$^2$, air pressure = 1.333 N/m$^2$, air density = $1.71 \times 10^{-5}$ kg/m$^3$, air kinematic viscosity coefficient = 1.17 m$^2$/s, coefficient of thermal-expansion for air $\beta = 2.87 \times 10^{-3}$ 1/K and Prandtl number for air = 0.72, heat conduction coefficient for air = $1.8 \times 10^{-2}$ J/(m s K), and the constant pressure specific heat, $c_p$, for air = $1.014 \times 10^3$ J/(kg K).

Based on a Boussinesq approximation, application of the thermal expansion formulation is appropriate due to the considerable temperature and density changes in the ampoule that arise from significant non-isothermal conditions. The most significant driving parameters in this study, avoiding an exhaustive discussion of dimensionless parameters, are the inertia, buoyancy and viscous terms,

$$ww/L \sim g_z \beta \Delta T \sim \nu w/\delta_T^2, \tag{17}$$

respectively, which are on the same order of magnitude in the momentum equation shown in Eq. (4); and convection and conduction terms,

$$w/L\Delta T \sim \alpha \Delta T/\delta_T^2, \tag{18}$$

respectively, which are also on the same order of magnitude in the energy equation shown in Eq. (5). Here, $\delta_T$ is the thermal boundary layer thickness; $L$ is the height of the container along the $z$-axis; $\nu = \mu/\rho$ is the kinematic viscosity; and $\alpha = k/\rho c_p$ is the thermal diffusivity. From convection and conduction terms in Eq. (18); from inertia and buoyancy terms in Eq. (17); and from buoyancy and viscous terms in Eq. (17), we can obtain convective velocity of flows as follows:

$$w \sim \alpha L/\delta_T^2, \tag{19}$$

$$w \sim (g_z \beta L \Delta T)^{1/2}, \tag{20}$$

$$w \sim (g_z \beta \delta_T^2 \Delta T)/\nu. \tag{21}$$

By equating Eqs. (19) and (21), we have the relationship

$$\delta_T/L \sim \mathrm{Ra}^{-1/4} \tag{22}$$

a result of the balance between buoyancy and viscous forces. By equating Eqs. (19) and (20), we have another relationship

$$\delta_T/L \sim (\mathrm{Ra\,Pr})^{-1/4} \sim (\mathrm{Gr})^{-1/4}(\mathrm{Pr})^{-1/2} \tag{23}$$

based on the balance between buoyancy and inertia forces. Here the Rayleigh number (Ra), Grashof number (Gr), and Prandtl number (Pr) are defined as

$$\mathrm{Ra} = g_z \beta L^3 \Delta T/\alpha\nu, \tag{24}$$

$$\mathrm{Gr} = g_z \beta L^3 \Delta T/\nu^2 = \mathrm{Ra}/\mathrm{Pr}, \tag{25}$$

and

$$\mathrm{Pr} = \nu/\alpha. \tag{26}$$

Since the heat transfer coefficient scales as $k/\delta_T$ [25], the Nusselt number (Nu) varies as

$$\mathrm{Nu} = hL/k \sim \mathrm{Ra}^{1/4} \tag{27}$$

from Eq. (22) based on the balance between buoyancy and viscous forces inside the thermal layer; and Nu varies as

$$\mathrm{Nu} \sim (\mathrm{Ra\,Pr})^{1/4} \sim (\mathrm{Gr})^{1/4}(\mathrm{Pr})^{1/2} \tag{28}$$

from Eq. (23) based on the balance between inertia and buoyancy forces inside the thermal layer. As indicated by Bejan [28] both theoretical and laboratory measurements show that Eq. (27) is particularly applicable for Pr > 1 fluids, while Eq. (28) is dominated by Pr ≪ 1 fluids. For the case of the present research, the dominant parameter is the Rayleigh number rather than Grashof number [28] since for air, Pr ≈ 1.

In this study, it is shown in the numerical simulation that for the range of parameters considered, the maximum induced flow velocity driven by convection is 0.165 m/s. The Reynolds number (Re =

$wD/\nu$, where $D$ is the diameter of the container) for the flow pattern based on this flow velocity is 0.025 m/s, which is far below the threshold for production of turbulent flow fields. The Grashof and Rayleigh numbers for the present case study are 0.0184 and 0.0133, respectively, for unit gravity. The aspect ratio of the reaction chamber (height : cross-sectional radius = 6 : 1.5) is sufficiently large such that any radial gradient $(T - T_z)$ will result in buoyancy-driven flows [28]. That is, there is no critical Rayleigh number requirement for the onset of convection in the present study.

## 4. Mathematical simulation of flow profiles and temperature distributions

Eqs. (1)–(5) subject to initial conditions shown in Eqs. (8)–(11), and boundary conditions shown in Eqs. (12)–(16), have been used to solve time-dependent, three-dimensional flow profiles and temperature distributions numerically. The computer algorithms employed in this study have been developed and illustrated in our earlier studies [29–39] and will not be repeated in this paper. The time step is determined automatically based on the size of grid points and the velocity of flow fields. Since the thickness of the boundary layer is inversely proportional to the square root of Reynolds number, the spacing is adjusted such that it decreases with increasing Reynolds number [40,41].

In this study, two sets of grids, with grid sizes $17 \times 34 \times 42$ and $23 \times 34 \times 82$ along $(r, \theta, z)$ coordinates, have been designed to carry out numerical computations. For a Reynolds number of 0.025 with maximum induced velocity of 0.165 m/s, as in the present case, there is concluded to be no difference for numerical results obtained for either grid chosen. By using the grids $17 \times 34 \times 42$ in the computation of flows with higher Reynolds number (such as

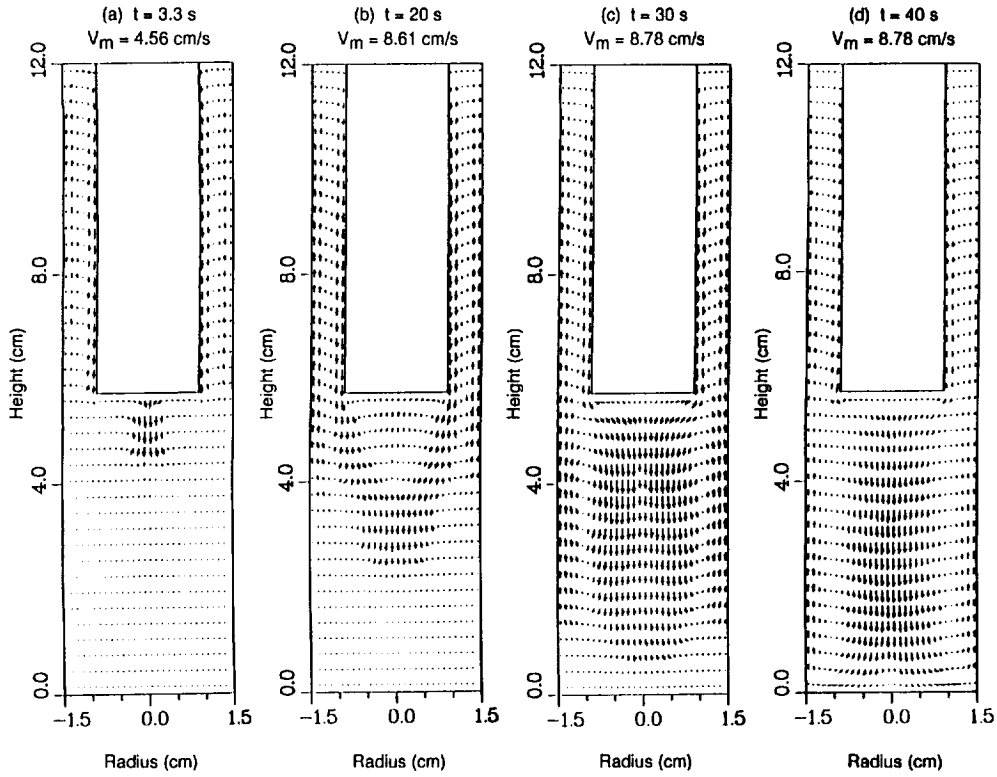


Fig. 2. Flow profile initiation and development along the $z$-axis parallel to the plane $\theta = 0°–180°$ and to gravitational acceleration ($\psi = 0°$).

Re ≥ 1500) and induced velocity of 1.66 m/s and higher, extremely severe numerical instabilities of the flow field result. With grids $17 \times 34 \times 42$, the average time step determined from the size of grid points and velocity of flow fields is 0.00076 s, while the CPU time required by the Supercomputer CRAY II to execute one time step is 3.019 s. The total CPU time consumed for each of the three cases in this study is 12 000 s. The cell orientation varies relative to gravity according to $\psi = 0°$, 45°, and 180°, by rotating the $z$-axis. We observe flow profiles in the cell in the orthogonal planes, $\theta = 0°–180°$ and $\theta = 90°–270°$ to investigate the characteristics of convection-driven flows and temperature profiles. Various references have been cited by Bejan [28] in the study of induced convective heat transfer with fluid layers heated from below, top, side, oblique, etc., under normal atmospheric pressure.

As mentioned in the Introduction, this study investigates the time dependence from initiation and development of flow fields and temperature distribution throughout the vapor deposition process. The objective is to determine the sensitivity of the formation of NLO thin films to convection in the relatively low pressure environment of $10^{-2}$ mm Hg. To our knowledge, there are no studies of induced convective heat transfer at relatively low pressure, hence, there is no available literature for comparison. However, the following discussion concludes there is qualitative agreement on flow profiles and temperature distribution for induced convection at both normal atmospheric pressure and $10^{-2}$ mm Hg.

## 5. Convection driven by processing with the cell oriented parallel ($\psi = 0°$) to gravitational acceleration

Fig. 2 shows the time dependency for the development of flow fields ($V_m$ = maximum velocity at time, $t$) upon bottom heating of the cell oriented in the direction parallel ($\psi = 0°$) to gravitational acceleration. Fig. 3 shows time animation of the initiation and formation of temperature profiles due to induced convection in the $r$–$z$ plane, parallel to the plane $\theta = 0°–180°$. The curves shown in Fig. 5 are the isothermal lines with temperatures in °C at the corresponding locations. Figs. 2 and 3 can be summarized as follows: (a) At time $t = 0$ (not shown), there is very sharp temperature variance from 30 to 120°C in

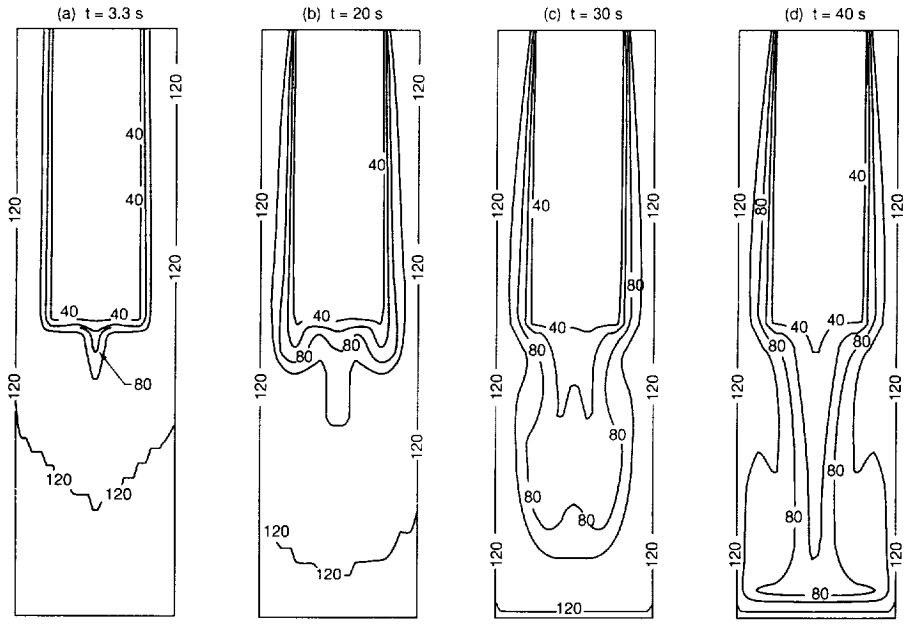


Fig. 3. Initiation and formation of the temperature profile along the $z$-axis parallel to the plane $\theta = 0°–180°$ and to gravitational acceleration ($\psi = 0°$).

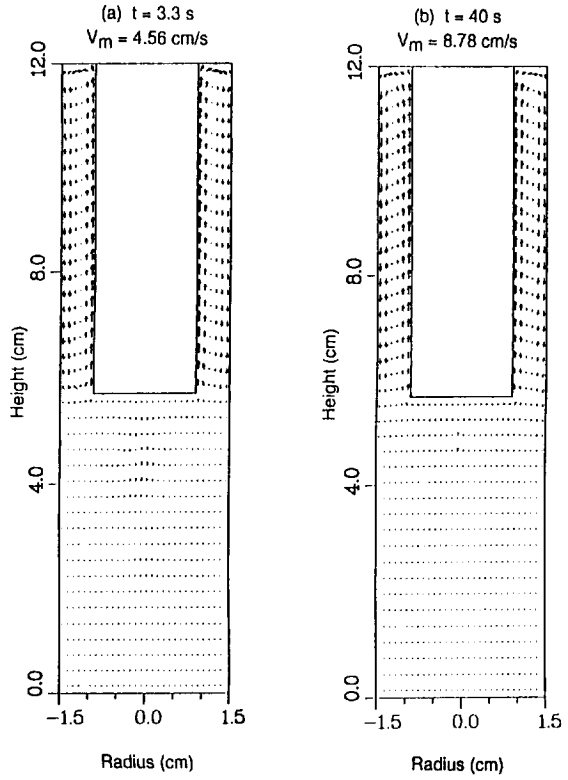


Fig. 4. Flow profile initiation and development along the $z$-axis parallel to the plane $\theta = 0°–180°$ with top heating ($\psi = 180°$).

a fairly thin layer. (b) An initiation of downward flow from the bottom of the central column toward the bottom of the outer cylinder immediately creates a gradually expanding positive temperature gradient along the downward directions for time $t > 1.5$ s. (c) A pattern of induced inflow from the surface of the outer cylinder toward the center promotes a parabolic temperature profile with the downside tip point around the center. This pattern is due to downward cold streams from the bottom of the central column for time $t > 1.5$ s. (d) An induced upward profile of temperature distribution around the surface of the outer cylinder is a result of an upward flow pattern along the corresponding surface. (e) A downward elongation profile of temperature distribution immediately around the neighborhood of the surface of the inner cylinder (central column). This pattern is a result of the induced downward flow along the corresponding surface.

## 6. Convection driven by processing with the cell oriented in the reverse parallel direction ($\psi = 180°$) to gravitational acceleration

Fig. 4 and Fig. 5 show the time dependency for the development of induced flow fields upon top heating of the cell oriented in the parallel direction ($\psi = 180°$) to gravitational acceleration. This problem can be divided into two sections. For $z > 6$ cm, the problem can be associated with horizontal heating from the outer walls of the cylinder toward the central wall within a narrow cylindrical slit of space. For $z < 6$ cm, the problem is that of vertical heating from the top (downward gravity direction). As the source material is located at the surface of $z = 0$ (now at the top), and the location of vapor deposition is at the bottom horizontal surface of the central column at $z = 6$ cm, the flow profile at $z > 6$ cm has very little effect on the flow pattern at the deposition surface. Thus, we can ignore the flow profiles induced within a narrow cylindrical slit of space. As to the flow at $z < 6$ cm, Fig. 4 shows a stable stratified

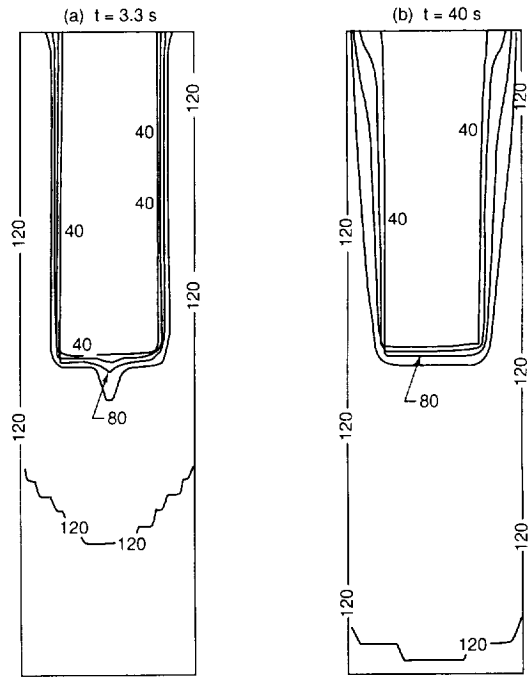


Fig. 5. Initiation and formation of the temperature profile along the $z$-axis parallel to the plane $\theta = 0°–180°$ with top heating ($\psi = 180°$).

medium and natural convection is absent provided there is no side heating.

Fig. 5 shows the time evolution of initiation and formation of temperature profiles for this case. The curves in Fig. 5 are the isothermal lines with temperature in °C at the corresponding locations. Again, the figure clearly shows two regions. For the region $z > 6$ cm, horizontal heating from the side walls drive the convective flow toward the central wall within a narrow cylindrical slit. Fig. 5 depicts a series of isothermal curves with decreasing temperature from the side wall toward the central column. As indicated earlier, this region is not important in our study of vapor deposition from source materials located on the surface at $z = 0$ and transferring to the bottom of the central column at $z = 6$ cm. There is not much variation in the dynamics of temperature distribution for the region $z < 6$ cm because the region is filled with the stable stratified medium, and natural convection is completely prohibited. Nevertheless, the heating and consequential flow transient is of interest.

## 7. Convection driven by the oblique direction at 45° to gravitational acceleration

In this case, the cell $z$-axis is allowed to tilt at 45° relative to gravitational acceleration parallel to the plane, $\theta = 0°–180°$. Fig. 6 illustrates convective flows induced by a vector summation of gravitational acceleration with a horizontal component at $0.707g_0$ ($g_0 \sin 45°$) rightward, and vertical component at $0.707g_0$ ($g_0 \cos 45°$) downward.

Comparison of Fig. 2 and Fig. 6, and Fig. 2 and Fig. 7 show the differences in induced flow fields in the $\theta = 0°–180°$ and $\theta = 90°–270°$ planes, respectively, driven by vertical and titled cavities. There are two recirculation flows generated with centers at $(r_c, z_c) = (\pm 1.90, 2.7)$ cm and at $(r_c, z_c) = (\pm 0.8, 3.2)$ cm for flows induced by vertical and tilted orientations, respectively. For the vertical orientation, the flow depicted in Fig. 2 is axisymmetric, hence also representative of flows in the $\theta = 90°–270°$ plane. The flows are upward along the surface of the outer cylinder and downward from the central column. These are Benard-type flows driven by counter-rotating cells (clockwise on the left and

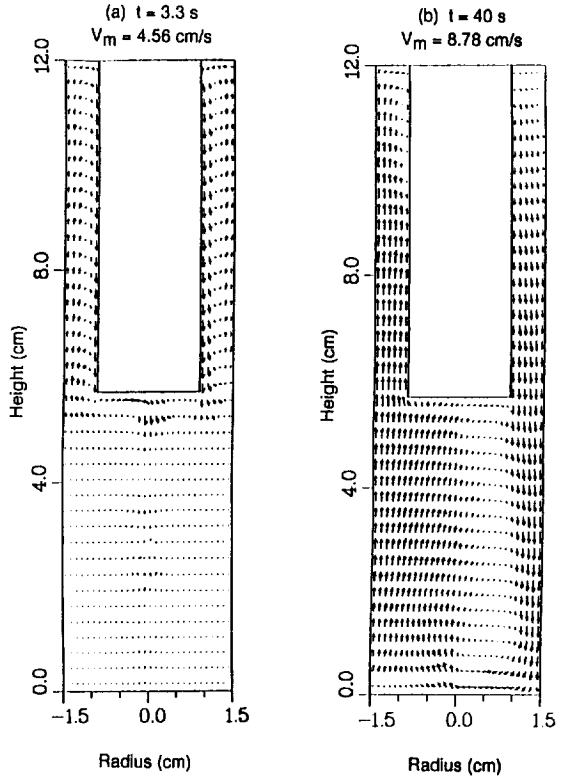


Fig. 6. Flow profile initiation and development along the $z$-axis parallel to the plane $\theta = 0°–180°$ and oblique to gravitational acceleration ($\psi = 45°$).

counter-clockwise on the right) due to an incipient instability in the narrow cylindrical cell cavity. There is no critical Rayleigh number for convection, which assumes an infinite extent of the cell width. For the tilted cell, a resultant asymmetric flow in the $\theta = 0°–180°$ plane approaches an antisymmetric flow profile resulting from differential heating between vertical and opposite walls of a cavity. That is, an incipient instability causes heat to flow along the bottom surface (now tilted upward), and upward along the side wall, and along the cold surface (downward), and downward along the other side wall. The two recirculation flows for this orientation appear in the $\theta = 90°–270°$ plane (Fig. 7). There is an upward flow from the bottom surface of the outer cylinder transporting heat toward the bottom surface of the central column with downward flows on the outside walls (clockwise on the right and counter-clockwise on the left). This asymmetric three-dimensional flow

profile is quite complex and represents a greater degree of convection in the cell cavity for the tilted orientation.

Fig. 8 and Fig. 9 show time evolution of the initiation and formation of temperature profiles along the $z$-axis parallel to $\theta = 0°–180°$ and $\theta = 90°–270°$, respectively. Fig. 8 depicts the temporal variation of isothermal lines as a result of the tilted orientation with respect to gravity. The isotherms are consistent with the motion of flow fields. Comparison of Fig. 6 for the velocity profile and Fig. 8 for the temperature profile demonstrates that the flow field affects the temperature field. Fig. 9 shows similar temporal variation of isothermal lines from another point of view. Initiation and development of a cone-shaped temperature profile is the result of direct upward flow from the bottom surface of the outer cylinder transporting heat toward the bottom surface of the central column. This is viewed in the $\theta = 90°–270°$ plane and is consistent with the flow profile in Fig. 7. These preliminary observations suggest that various convection patterns can affect film thickness and quality during deposition by vapor transport.

## 8. Near ultraviolet / visible absorbance spectra of vapor deposited diacetylene-MNA (DAMNA) films as a function of cell orientation

In this work, it is helpful to utilize Beer–Lambert's relationship for transmission of radiation through a medium to test gravitationally sensitive flow pattern predictions. We would expect that the flow pattern in Fig. 7 (cell tilted at 45° relative to gravity vector) would affect film quality over most of the deposition surface differently than the flow pattern depicted in Fig. 2 (cell oriented parallel to gravity vector). Preliminary experiment suggests this to be the case with

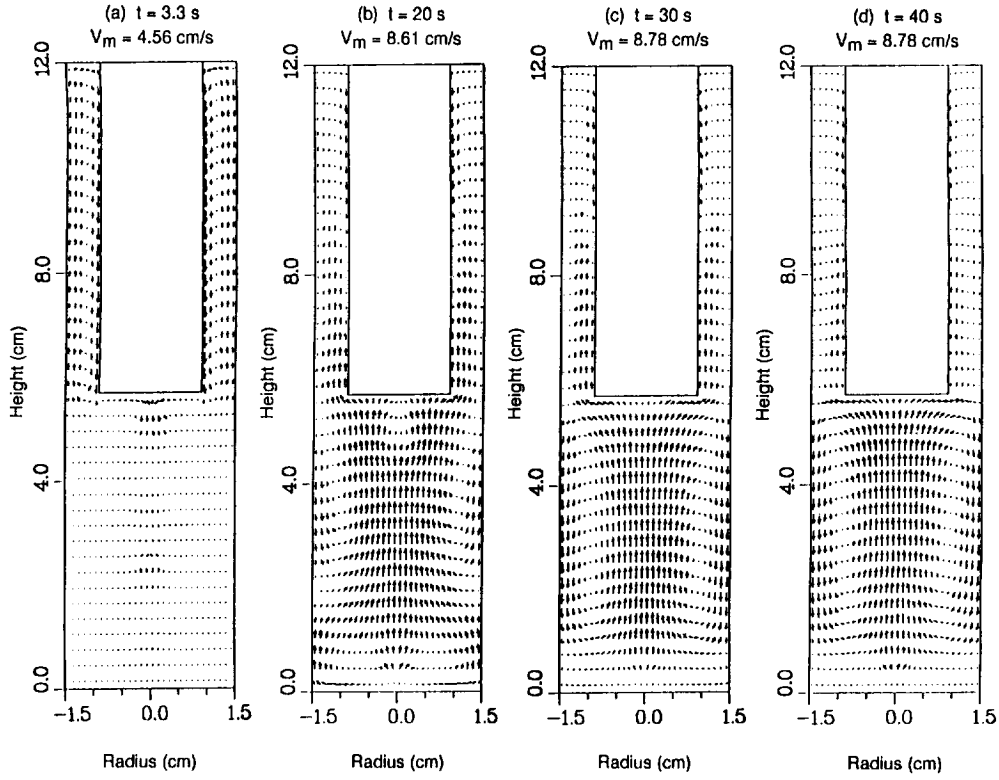


Fig. 7. Flow profile initiation and development along the $z$-axis parallel to the plane $\theta = 90°–270°$ and oblique to gravitational acceleration ($\psi = 45°$).

respect to film thickness. The Beer–Lambert law relative to film thickness can be written

$$I = I_0 e^{-\alpha \ell}, \tag{29}$$

where $I_0$ is incident radiation intensity, $I$ is the reduced radiation intensity after passing through the film, $\alpha$ a proportionality constant containing the molar absorption coefficient, $\epsilon$, and concentration of absorber, and $\ell$ is film thickness. The molar absorption coefficient represents a molar cross section for absorption. The greater the cross section of the molecule for absorption and absorber concentration, the greater the attenuation of the intensity of the beam. Likewise, film thickness, $\ell$ also attenuates the beam intensity accordingly. The ratio $I/I_0$ is a measure of beam transmittance, $T$. We would expect a larger intensity in the absorption bands of films deposited in cells tilted at 45° over those where deposition occurred in cells positioned vertically. We may define the dimensionless product $A = -\alpha\ell$ as absorbance, which incorporates all of the contributors to beam attenuation. Since the nature of the material, DAMNA, and concentration (pure material) are identical in both cases, then absorbance is only a function of film thickness. Fig. 10a is a wavelength scan in the range 190 to 820 nm of a vertically deposited film, and Fig. 10b is that of an obliquely deposited film. Table 1 contains representative absorbance intensities from scanning an approximately 1 cm diameter spot in similar vicinities of films formed during vapor deposition in vertically and obliquely oriented cells. Visually, the films from the obliquely oriented cells are a deeper yellow color than those from vertically oriented cells. We qualitatively assume generally thicker films from the relative appearances. The surfaces of these monomer films are translucent and microcrystalline. At the present time, it is also preferable for us to discuss relative film thickness from beam attenuation in qualitative terms (although more quantitative than visual observation) while observing that the spectroscopic irradiation spot sizes are large enough to average over about 50% of the film surfaces. The same relative result occurred, in that beam attenua-

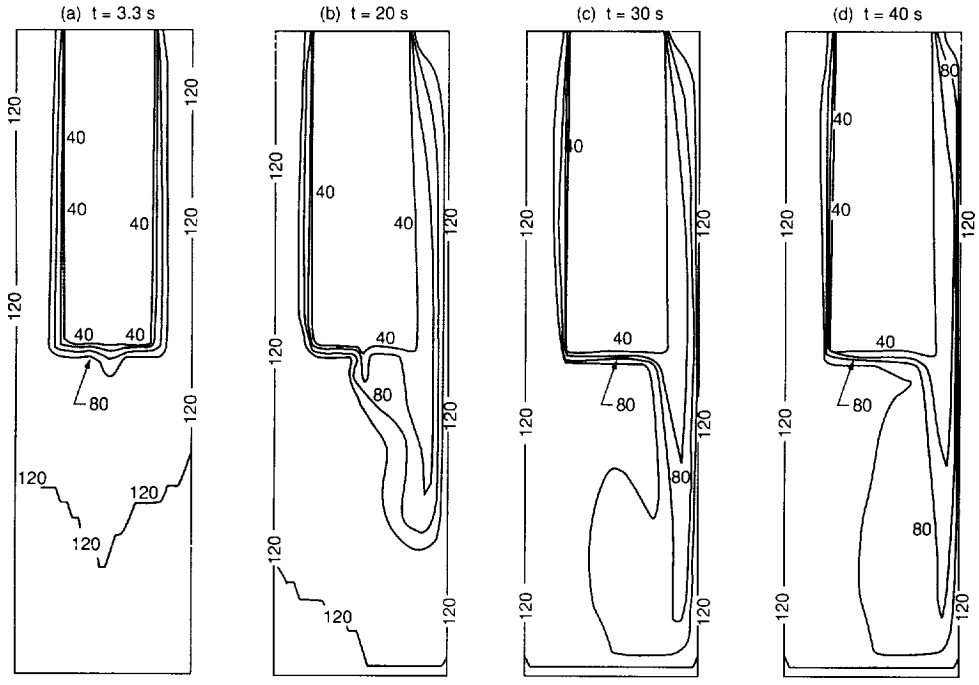


Fig. 8. Initiation and formation of temperature profile along the z-axis parallel to the plane $\theta = 0°–180°$ and oblique to gravitational acceleration ($\psi = 45°$).

tion was greater at each maximum absorbance wavelength repeatedly. We may consider Table 1 a qualitative representation of a consistent result. Depositions were of 30 min duration. Cell dimensions were the same as those discussed in the modeling section. The cells were pumped to $10^{-2}$ mm pressure prior to deposition, and sealed. Without the presence of DAMNA in the vessel, appreciably lower total pressures are obtainable. We may infer that the evacuation pressure reaches a minimum because of the vapor pressure of DAMNA, which will be equal to, or greater than, the evacuation pressure, $10^{-2}$ mm. From a different study, the measured vapor pressure of 4-N,N-dimethylamino-4'-nitrostilbene (DANS) at 120°C was reportedly 0.374 mm [42]. This is a relatively large organic molecule having a molecular weight of 211 g/mol as compared to DAMNA with a molecular weight of 247 g/mol. Considering structural and size similarities, we may approximate similarities in vapor pressure. Indeed, heptadecanol (molecular weight = 256.5 g/mol), also an alcohol with possible hydrogen bonding in its condensed phases such as expected of DAMNA, has a vapor pressure of $10^{-1}$ mm at 120°C [43]. There is no reason to expect DAMNA to differ drastically from these measured vapor pressures, and we may approximate that the vessel evacuation pressure minimum is largely due to the vapor pressure of DAMNA.

The vacuum was virtually unchanged during deposition. The oil baths circulated at 120 and 30°C (source and sink, respectively) prior to allowing flow into the experimental cell. The temperature differentials between the baths and respective oil jackets of the experimental cells were small (~ 2°C). This allowed operation during deposition at constant heat fluxes of ~ 120°C at the source and ~ 30°C at the sink, consistent with theoretical conditions. Since the mathematical formulations only considered the thermal flow profiles using air data, these results are estimates. That is, the effects of mass transport are not included in these assessments. However, at low pressures and moderately high temperatures, we can expect ideal gas behavior as a first approximation; namely, that gaseous molecules are essentially point masses. In comparing experiment with the model, we expect that heats of sublimation and condensation will have little effect on the thermal profile. Vapor phase estimates on the basis of ideal gas considerations and DAMNA condensed volume, places DAMNA's mole fraction in the available cell cavity to be very high relative to air (~ 1). The model material parameters for air predict the effect of kinematic viscosity to be of the same order as thermal diffusivity, which is the case for $Pr \approx 1$ fluids (Eq. (26)). The classical heat capacity for a gaseous molecule, such as DAMNA, with its large number of vibrational degrees of freedom, is only achieved at high temperatures. That is, the heat capacity of DAMNA will approach that of a diatomic molecule, such as the major components of air, since its vibrational modes are unable to store energy at these low temperatures. The thermal diffusivity approximation using air data is, therefore, a fair one assuming

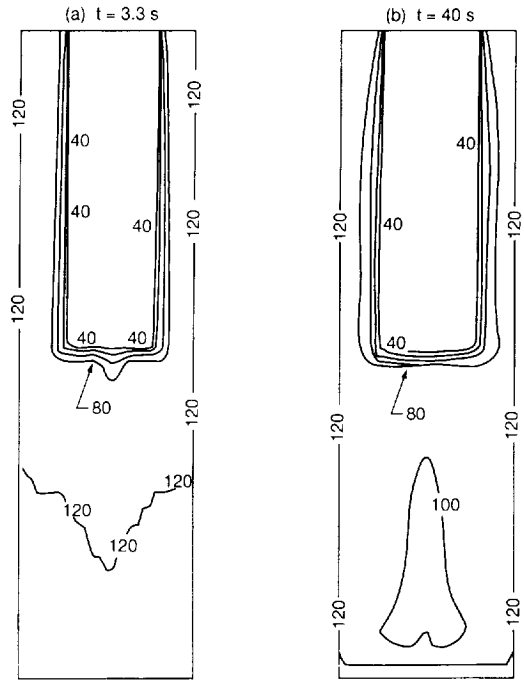


Fig. 9. Initiation and formation of temperature profile along the z-axis parallel to the plane $\theta = 90°–270°$ and oblique to gravitational acceleration ($\psi = 45°$).

Table 1
Representative absorbance intensities of deposited films

| $\lambda$ (nm) | $A_{max}$ (cell vertical film) | $A_{max}$ (cell oblique film) |
|---|---|---|
| 422 | 0.200 | 0.385 |
| 214 | 0.395 | 0.546 |

similar heat conduction coefficients. In the classical limit, the higher heat capacity would yield $Pr \gg 1$. Because an ideal heat capacity approximation is an overestimate at the operating temperatures, deviation from ideal behavior causes $Pr \approx 1$, closer to that of air. Without actual data for DAMNA, we are left with experimental data from the low operating pressures and temperatures to compare with modeling estimates. Close agreement between experiment and the model would indicate that DAMNA at these pressures indeed approximates an ideal gas with the appropriate deviations which tend toward validation of the use of air physical constants. Furthermore, the constant heat flux provided by the circulating bath is a factor in neutralizing thermal effects specific to individual molecules. In keeping with the assump-

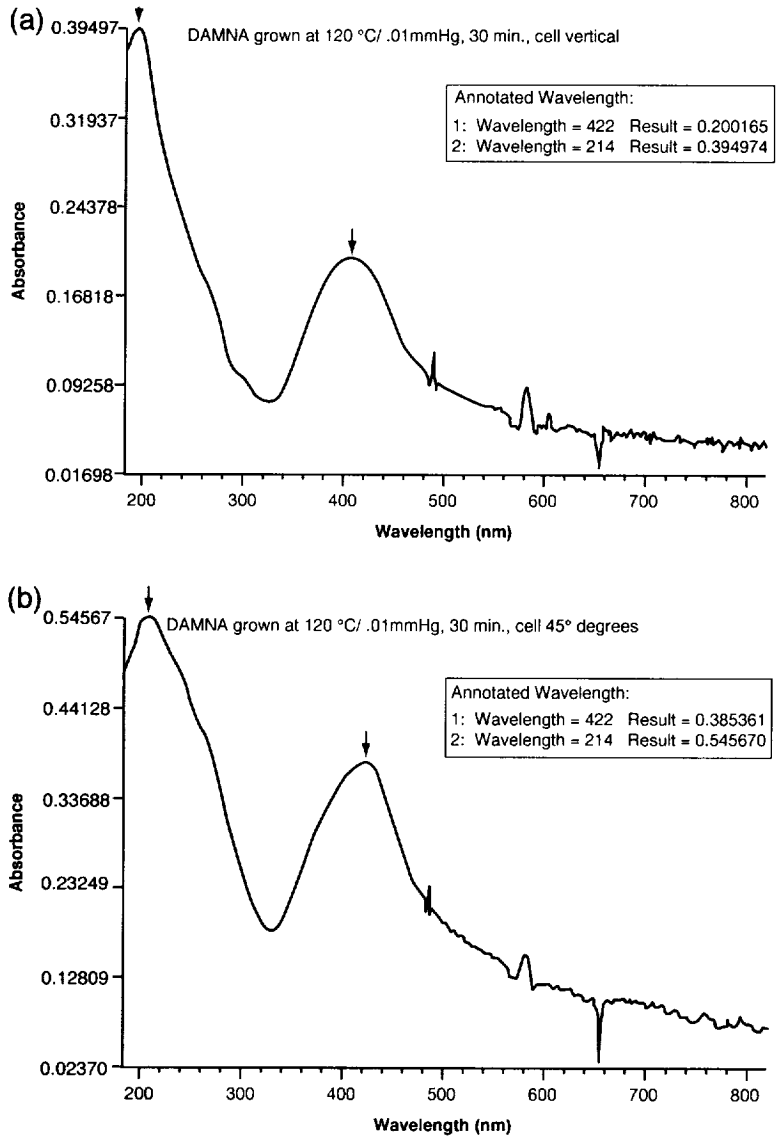


Fig. 10. Representative ultraviolet/visible spectrum of a deposited DAMNA film in (a) the deposition cell oriented vertically with respect to the gravity vector, and in (b) the deposition cell oriented at 45° with respect to the gravity vector.

tions, the mathematical model correctly predicts qualitative differences in film properties between vertically and obliquely oriented cells. That is, more convection in cells having the tilted orientation is apparently responsible for correspondingly greater film thickness. Future work will strive to correlate experimental kinetics of film growth with calculated heat and mass transfer rates.

## 9. Discussion and conclusion

The purpose of the present study is to investigate heat transfer characteristics in an ideal gas in a thermal gradient at relatively low pressure and various orientations with respect to the gravity vector. Mathematical formulations yield fluid profiles, air and temperature distributions driven by heat transfer processes during natural convection at orientations parallel and oblique with respect to gravity. Several experiments to grow films by PVT have resulted in some controversy. The argument raises the question of minimum pressure levels for convection to be a factor. Neither has it been clear as to the types of convection which might occur during PVT that would affect the quality, homogeneity and orientation of vapor deposited films as in the 3M microgravity experiment. Mechanisms thus described to discuss the 3M experiment are generally in terms of thermal stress and creep due to high horizontal thermal gradients at the corners and thermal gradients along the walls [44]. Although our ground-based experiment only roughly approximates PVTOS, Fig. 8 illustrates the presence of such gradients in an $r$–$z$ plane parallel to the plane, $\theta = 0°$–$180°$.

In this study, numerical computation of a full set of nonlinear fluid dynamical equations show that the vapor deposition process has to be accomplished through a fairly complicated set of flow patterns (particularly for three-dimensional flows at $\psi = 45°$) of recirculation in unit gravity at pressures as low as $10^{-2}$ mm Hg. Since these equations also demonstrate an enhancement of convection as we move from vertical to oblique orientation of the cell with respect to the gravity vector, it is feasible to apply a simple preliminary test of these calculations by macroscopic assessments of film quality of vapor deposited films in respectively oriented cells. The preliminary experimental result tends to support the numerical computations.

## Acknowledgements

The authors gratefully recognize NASA support through the Cooperative Agreement No. NCC8-38, and the helpful suggestions of I. Alexander.

## References

[1] B.K. Nayar and C.S. Winter, Opt. Quantum Electron. 22 (1990) 297.
[2] G.M. Carter, Y.J. Chen and S.K. Tripathy, Appl. Phys. Lett. 43 (1988) 891.
[3] F. Kajzar, J. Meissier, J. Zyss and I. Ledoux, Opt. Commun. 45 (1983) 133.
[4] F. Kajzar and J. Messler, Thin Solid Films 11 (1988) 132.
[5] M. Thakur and S. Meyler, Macromolecules 18 (1985) 2341.
[6] M. Thakur, G.M. Carter, S. Meyler and H. Hryniewicz, Polymer Preprints 27 (1986) 49.
[7] I. Ledoux, D. Josse, P. Vidakovic and J. Zyss, Opt. Eng. 27 (1986) 49.
[8] M.S. Paley, D.O. Frazier, S.P. McManus, S.E. Zutaut and M. Sangahadasa, Chem. Mater. 5 (1993) 1641.
[9] M.K. Debe and K.K. Kam, Thin Solid Films 186 (1990) 289.
[10] D.O. Frazier, B.G. Penn, W.K. Witherow and M.S.Paley, SPIE Cryst. Growth Space Relat. Diagnostics 1557 (1991) 8697.
[11] G.Z. Wegner, Naturforsch. 246 (1969) 824.
[12] M.K. Debe, Progr. Surf. Sci. 24 (1987) 1.
[13] C.J. Liu, M.K. Debe, P.C. Leung and C.V. Francis, Appl. Phys. Commun. 11 (1992) 151.
[14] K.K. Kam, M.K. Debe, R.J. Poirier and A.R.Drube, J. Vac. Sci. Technol. A 5 (1987) 1914.
[15] M.K. Debe, K.K. Kam, C.J. Liu and R.J. Poirier, J. Vac. Sci. Technol. A 6 (1988) 1907.
[16] M.K. Debe, J. Appl. Phys. 55 (1984) 3354; M.K. Debe and T.N. Tommet, J. Appl. Phys. 62 (1987) 1546.
[17] M.K. Debe, R.J. Poirier and K.K. Kam, Thin Solid Films 197 (1991) 335.
[18] M.K. Debe and D.R. Field, J. Vac. Sci. Technol. A 9 (1991) 1265.
[19] M.K. Debe, J. Vac. Sci. Technol. A 10 (1992) 2816.
[20] M.K. Debe, J. Vac. Sci. Technol. 21 (1992) 74.
[21] M.K. Debe, R.J. Poirier, D.D. Erickson, T.N. Tommet, D R. Field and K.M. White, Thin Solid Films 186 (1990) 257.
[22] M.K. Debe and R.J. Poirier, Thin Solid Films 186 (1990) 327.
[23] H.A. Abdeldayem, D.O. Frazier, B.G. Penn, W.K. Witherow, C. Banks, A. Shields and R. Hicks, Appl. Phys. Lett., submitted.

[24] G.H. Westphal and F. Rosenberger, J. Crystal Growth 43 (1978) 687.
[25] D.W. Greenwell, B.L. Markham and F. Rosenberger, J. Crystal Growth 51 (1981) 413.
[26] B.L. Markham, D.W. Greenwell and F. Rosenberger, J. Crystal Growth 51 (1981) 426.
[27] M.S. Paley, D.O. Frazier, H. Abdeldayem, S.P. McManus and S.E. Zutaut, J. Am. Chem. Soc. 114 (1992) 3247.
[28] A. Bejan, Convection Heat Transfer, 2nd ed. (Wiley, New York, 1995) p. 623.
[29] R.J. Hung, K.L. Shyu and C.C. Lee, J. Propulsion Power 8 (1992) 778.
[30] R.J. Hung, K.L. Shyu and C.C. Lee, J. Spacecraft Rockets 29 (1992) 523.
[31] R.J. Hung, C.C. Lee and F.W. Leslie, J. Guidance Control Dynamics 15 (1992) 817.
[32] R.J. Hung, C.C.Lee and F.W. Leslie, J. Fluids Struct. 6 (1992) 493.
[33] R.J. Hung, C.C. Lee and F.W. Leslie, Trans. Jpn. Soc. Aeronautical Space Sci. 35 (1993) 187.
[34] R.J. Hung, C.C. Lee and F.W. Leslie, J. Aerospace Eng. 207 (1993) 105.
[35] R.J. Hung, H.L.Pan and F.W. Leslie, Fluid Dynamics Res. 14 (1994) 29.
[36] R.J. Hung, H.L. Pan and F.W. Leslie, J. Flight Sci. Space Res. 18 (1994) 195.
[37] R.J. Hung, H.L. Pan and Y.T. Long, Acta Mech. Sin. 10 (1994) 367.
[38] R.J. Hung, H.L. Pan and Y.T. Long, Cryogenics 34 (1994) 641.
[39] R.J. Hung, Y.T. Long and H.L. Pan, Trans. Jpn. Soc. Aeronautics Space Sci. 37 (1994) 217.
[40] C.W. Kitchens, N. Gerber and R. Sedney, J. Spacecraft Rockets 15 (1978) 348.
[41] C.W. Kitchens Jr., AIAA J. 18 (1980) 929.
[42] M. Zugrav, private communication.
[43] R.C. Reid, J.M. Prausnitz and B.E. Poling, The Properties of Gases and Liquids, 4th ed. (McGraw-Hill, New York, 1987).
[44] D.E. Rosner, Phys. Fluids A 1 (1989) 1871.

# Journal of Crystal Growth

## Instructions to Authors (short version)

**Submission of papers**
Manuscripts (one original + two copies), should be sent to a member of the Editorial Board or preferably to an appropriate subject Associate Editor. News or announcements should be submitted through the Principal Editor; a duplicate should be sent directly to Elsevier Science B.V., address given below.
*Original material.* Submission of a manuscript implies it is not being simultaneously considered for publication elsewhere and that the authors have obtained the necessary authority for publication.

**Types of contributions**
Original research papers, Letters to the Editors and Priority communications are welcome. They should contain an Abstract (of up to 200 words) and a Conclusions section, which particularly in the case of theoretical papers translates the results into terms readily accessible to most readers.
As a guideline: *experimental papers* should not be longer than 16 double-spaced typed pages, and 8 figures + tables; for *theoretical papers* a maximum of 20 pages and 10 figures + tables is suggested.
*Letters* and *Priority communications* should not be longer than 5 double-spaced typed pages, and 3 figures + tables. They will be given priority in both the refereeing and production processes. The faster production schedule may preclude sending proofs of Letters and Priority communcations to authors.

**Manuscript preparation**
Contributions may be written in English, French or German. They should have an abstract in English. The paper copies of the text should be prepared with double line spacing and wide margins, on numbered sheets.
*Structure.* Please adhere to the following order of presentation: Article title, Author(s), Affiliation(s), Abstract, PACS codes and keywords, Main text, Acknowledgements, Appendices, References, Figure captions, Tables.
*Corresponding author.* The name, complete postal address, telephone and fax numbers and the e-mail address of the corresponding author should be given on the first page of the manuscript.
*Classification codes/keywords.* Please supply one to four classification codes (PACS and/or MSC) and up to six keywords of your own choice that descibe the content of your article in more detail.
*References.* References to other work should be consecutively numbered in the text using square brackets and listed by number in the Reference list. Please refer to the more detailed instructions for examples.

**Illustrations**
Illustrations should also be submitted in triplicate: one master set and two sets of copies. The *line drawings* in the master set should be original laser printer or plotter output or drawn in black india ink, with careful lettering, large enough (3–5 mm) to remain legible after reduction for printing. The *photographs* should be originals, with somewhat more contrast than is required in the printed version. They should be unmounted unless part of a composite figure. Any scale markers should be inserted on the photograph itself, not drawn below it.
*Colour plates.* Figures may be published in colour, if this is judged essential by the Editor. The Publisher and the author will each bear part of the extra costs involved. Further information is available from the Publisher.

**After acceptance**
*Important.* When page proofs of the accepted manuscripts are made and sent out to authors, this is in order to check that no undetected errors have arisen in the typesetting (or file conversion) process. At the proof stage only printer's errors may be corrected. No changes in, or additions to, the edited manuscript will be accepted.
*Notification.* The authors will receive the final answer of acceptance or rejection from the Office of the Principal Editor and will be invited to supply an electronic version of the accepted text, if this is not already available.
*Copyright transfer.* In the course of the production process you will be asked to transfer the copyright of the article to the Publisher. This transfer will ensure the widest possible dissemination of information.

**Electronic manuscripts**
The Publisher welcomes the receipt of an electronic version of your accepted manuscript. If there is not already a copy of this (on diskette) with the journal editor at the time the manuscript is being refereed, you will be asked to send a file with the text of the accepted manuscript directly to the Publisher by e-mail or on diskette (allowed formats 3.5" or 5.25" MS-DOS, or 3.5" Macintosh) to the address given below. (When e-mailing a non-ASCII word-processor file, you should encode it, e.g. with UUENCODE or BinHex, so as to retain all formatting codes.) The name and version of the word-processing program and the type of operating system should always be indicated. Please note that no deviations from the version accepted by the Editor of the journal are permissible without the prior and explicit approval by the Editor. Such changes should be clearly indicated on an accompanying printout of the file.

**Author benefits**
*No page charges.* Publishing in Journal of Crystal Growth is free.
*Free offprints.* The corresponding author will receive 50 offprints free of charge. An offprint order form will be supplied by the Publisher for ordering any additional paid offprints.
*Discount.* Contributors to Elsevier Science journals are entitled to a 30% discount on all Elsevier Science books.

**Further information (after acceptance)**

Elsevier Science B.V., J. Crystal Growth
Issue Management Physics
and Materials Science
P.O. Box 2759, 1000 CT Amsterdam
The Netherlands
Fax: +31 20 485 2319/+31 20 485 2704
E-mail: matsci-de-f@elsevier.nl

North-Holland, an imprint of Elsevier Science